RSC Advances

ROYAL SOCIETY OF CHEMISTRY

PAPER

View Article Online
View Journal | View Issue

Check for updates

Cite this: *RSC Adv.*, 2022, **12**, 24107

Colorimetric screening of elevated urinary mercury levels by a novel Hg^{2+}-selective probe of resorufin phosphinothioate†

Myung Gil Choi, Byung Hoon Yun, Hyeong Min Kim, Sangdoo Ahn * and Suk-Kyu Chang *

Urinary mercury levels are the most reliable indicators of mercury exposure but identifying them requires complex techniques and heavy instruments. In this research, we reported a simple and convenient urinary mercury analysis method using a readily available office scanner. Probe **MP-1** synthesized by the reaction of resorufin and dimethylthiophosphinoyl chloride revealed Hg^{2+}-selective chromogenic and fluorescent signaling behavior. Signaling was realized through Hg^{2+}-induced deprotection of the phosphinothioate protecting group in the resorufin-based probe **MP-1** to yield the parent fluorochrome. A pronounced colorimetric response of color change from light yellow to pink alongside a turn-on type fluorescence enhancement was perceived exclusively toward Hg^{2+} ions over other metal ions and anions. The colorimetry provided a more advantageous ratiometric approach than the simple fluorometric analysis exhibiting an off–on type response, with a detection limit of 12 nM (2.4 ppb). The Hg^{2+} signaling of the **MP-1** probe was not disturbed by the presence of coexisting metal ions and anions. The sensitive and convenient diagnosis of clinically important neurological symptoms and fatal inorganic mercury levels in urine was successfully demonstrated using a standard office scanner.

Received 2nd July 2022
Accepted 12th August 2022

DOI: 10.1039/d2ra04093j

rsc.li/rsc-advances

Open Access Article. Published on 24 August 2022. Downloaded on 2/11/2026 12:12:11 PM.
This article is licensed under a Creative Commons Attribution-NonCommercial 3.0 Unported Licence.

1. Introduction

Monitoring and removal of harmful water contaminants from polluted water are important since water pollution has become a serious environmental problem in our heavily industrialized society.[1–3] Emissions of toxic pollutants, including inorganic, heavy metal, and organic contaminants, are increased substantially by various chemical and related fields such as refinery, smelter, fertilizer, pulp, and pharmaceutical industries.[4] In particular, mercury is one of the most hazardous inorganic pollutants currently causing great concern in modern society and attracting much global attention for its negative impacts on our health and environment.[5] It exhibits highly bioaccumulative properties in the food chain, producing mostly neurological and immune system damage.[6] Mercury has many industrial applications, from the manufacturing of fluorescent light bulbs, jewelry, thermometers, and sphygmomanometers, in addition to cosmetics, insecticides, and pharmaceuticals.[7] Currently, a pressing concern for workers in mercury-exposed sectors is the prevention and remediation of mercury poisoning.[8] Mercury, which may be absorbed in inorganic and organic forms, is transformed into the most prevalent form of Hg^{2+} ions and can accumulate in the body of both humans and animals.[9] Even modest levels of Hg^{2+} poisoning can harm human health by causing damage to the brain and kidneys, as well as endocrine and neurological systems.[10,11] Consequently, the selective and sensitive quantification of trace mercury in both environmental and biological systems is a critical issue.

Blood, urine, hair, or fingernail samples are commonly used for clinical mercury analyses.[12] Commonly, urine samples have been widely employed as a viable biomarker for assessing the risk of exposure to mercurial species because their collection and management are non-invasive and simple.[13] Since inorganic mercury species are absorbed and deposited mostly in the proximal tubules of the kidneys, urinary mercury levels are one of the most acceptable indicators of chronic and acute exposure.[14] According to a recent study, the average mercury content in the urine of mercury-exposed miners was over 75 times higher than the control groups. The exposed miners suffered typical symptoms of mercury intoxication: digestive issues, hypomnesia, sleeping problems, tremors, and weight loss.[15] It is well known that urinary mercury concentrations greater than 100 μg L^{-1} cause neurological symptoms, whereas concentrations exceeding 800 μg L^{-1} are frequently linked to mortality.[16]

Many standard analytical techniques have been employed to determine elevated mercury concentrations in urine samples, including cold-vapor atomic-absorption spectrometry,[17]

Department of Chemistry, Chung-Ang University, Seoul 06974, Republic of Korea. E-mail: sangdoo@cau.ac.kr; skchang@cau.ac.kr; Fax: +82 2 825 4736; Tel: +82 2 820 5199

† Electronic supplementary information (ESI) available: UV-vis, fluorescence, and HPLC data, Hg^{2+} assay in artificial urine sample, ^{1}H and ^{13}C NMR spectra of probe **MP-1**. See https://doi.org/10.1039/d2ra04093j

© 2022 The Author(s). Published by the Royal Society of Chemistry

Open Access Article. Published on 24 August 2022. Downloaded on 2/11/2026 12:12:11 PM.
This article is licensed under a Creative Commons Attribution-NonCommercial 3.0 Unported Licence.

inductively coupled plasma mass spectrometry,[18] surface-enhanced Raman scattering,[19] bioluminescence,[20] and voltammetry.[21] Despite their great sensitivity and specificity for measuring mercurial species, these methods necessitate costly equipment, time-consuming sample preparation, and highly trained staff, and they can exhibit cross-sensitivity to other metal ions. Therefore, they might not be suitable for the convenient, selective, and sensitive on-site detection of Hg^{2+} ions. Consequently, it remains desirable to implement a simple, direct, and low-cost approach, such as optical sensors and molecular probes that create optical responses induced by the binding and/or reaction event for detecting Hg^{2+}.[22,23] In light of these, many colorimetric and/or fluorescence-based probes for the determination of urinary mercury levels have been reported. For example, carbothiohydrazide-appended diphenyl ether,[24] thiocarbonate derivative of perylene diimide dye,[25] dithioacetal derivative of bithiophene fluorophore,[26] and terbium complex of 7-amino-4-methyl-2(1*H*)-quinolinone[27] have been exploited for the urinary mercury detection. In addition, carbon dots,[28] DNA templated gold nanoparticles, and gold nanoclusters have also been developed for the determination of Hg^{2+} ions in urine samples.[29,30] A summary of the urinary mercury sensing system based on colorimetric and/or fluorescence signaling is presented in Table S1 (ESI†).

Recently, many elaborately designed optical sensors[31] and reaction-based small molecule probes have been developed to selectively and sensitively determine Hg^{2+} ions.[32,33] In particular, reaction-based probes relying on specific reactions with Hg^{2+} ions, such as Hg^{2+}-induced ring-opening reactions of rhodamine and fluorescein dyes,[34] protection–deprotection processes of phenolic dyes and aldehyde/ketone groups,[35] and desulfurization of thiocarbonyl functions, have been consistently developed.[36] We focused on the development of a reaction-based probe for Hg^{2+} ions, utilizing the specific and mild deprotection property of the phosphinothioate group. The phosphinothioate function has been exploited as a useful protection group for the phenol, thiol, and tryptophan groups in solid-phase peptide synthesis.[37,38] Mercury, silver, and fluoride ions have been effectively employed in the deprotection of these phosphinothioate-protected derivatives.[39] However, it has rarely been used to develop optical probes to analyze metal ions, anions, or other important industrial, environmental, and biological species.[40–43] Interestingly, the thiophosphoryl-containing compounds have similar stability to their phosphoryl analogs, which contrasts the significantly enhanced reactivity of thiocarbonyl compounds when compared to their analogous carbonyl derivatives.[44] Additionally, thiophosphoryl derivatives having the P═S function possess the ability to form complexes with softer metal ions.[45] We believe that the stability against spontaneous hydrolysis and softer ligating nature of the phosphinothioate group are advantageous features for a reaction-based probe to analyze thiophilic Hg^{2+} ions.

Here, we developed a simple colorimetric method focusing on the easy determination of urinary mercury concentrations. For the convenient detection of Hg^{2+} ions, a novel reaction-based dual signaling probe was synthesized by employing well-established resorufin as a signaling fluorochrome and a phosphinothioate protection group as a signaling switch. The probe showed selective and sensitive colorimetric and fluorogenic signaling properties exclusively toward Hg^{2+} ions. As a practical application, we could easily determine the two clinically relevant urinary mercury levels causing neurological symptoms (>100 ppb of Hg^{2+}) or leading to fatality (>800 ppb of Hg^{2+}). Furthermore, the sensitive and convenient diagnosis of these clinically crucial inorganic mercury levels in urine was successfully demonstrated using a typical office scanner without resorting to complicated instruments.

2. Experimental

2.1 Synthesis of MP-1

Resorufin sodium salt (470 mg, 2.0 mmol) was dissolved in *N*,*N*-dimethylformamide (DMF, 24 mL), before triethylamine (TEA, 540 μL, 4.0 mmol) was added to the mixture. After 30 minutes, dimethylthiophosphinoyl chloride (380 μL, 3.0 mmol) was added to the reaction pot and mixed for 12 hours at room temperature. Deionized (DI) water (50 mL) was added to the reaction mixture, and the resulting precipitate was filtered. The solid was dissolved in dichloromethane (DCM) and washed with DI water several times. The DCM phase was collected and dried with anhydrous $MgSO_4$. The solvent was evaporated under reduced pressure, and the remnant was purified by column chromatography (silica gel, eluent: DCM) to yield scarlet powder (0.50 g, 82%). ^{1}H NMR (600 MHz, DMSO-d_6) δ 7.87 (dd, J = 8.7, 0.7 Hz, 1H), 7.56 (d, J = 9.8 Hz, 1H), 7.39 (dd, J = 2.5, 1.6 Hz, 1H), 7.28 (ddd, J = 8.7, 2.6, 1.4 Hz, 1H), 6.83 (dd, J = 9.8, 2.1 Hz, 1H), 6.31 (d, J = 2.1 Hz, 1H), 2.11 (d, J = 13.5 Hz, 6H); ^{13}C NMR (150 MHz, $CDCl_3$) δ 186.1, 153.8 (d, J = 9.4 Hz), 149.9, 148.2, 144.6 (d, J = 1.5 Hz), 135.5, 135.0, 131.4 (d, J = 1.4 Hz), 130.9 (d, J = 1.9 Hz), 120.1 (d, J = 4.6 Hz), 109.9 (d, J = 5.0 Hz), 106.5, 23.9 (d, J = 71.7 Hz); HRMS (FAB); m/z calcd for $C_{14}H_{13}NO_3PS$ $[M + H]^+$: 306.0348, found 306.0351.

2.2 Preparation of stock solutions

A stock solution of probe **MP-1** (0.50 mM) was prepared in acetonitrile. Stock solutions of metal ions of perchlorate salt and sodium salt-containing anions (10.0 mM) were made by dissolving in DI water. A phosphate-buffered saline (PBS) solution (pH 7.4) was made according to a previous method.[46]

2.3 Preparation of Hg^{2+} sensing samples

The analytes for the Hg^{2+} sensing of **MP-1** were prepared in an optimized condition of PBS solution (pH 7.4) containing 20% acetonitrile. The metal ion or anion stock solution (30 μL, 10.0 mM) was added to a 15 mL vial and diluted successively with 2.22 mL of DI water and 0.57 mL acetonitrile. Then, solutions of PBS (0.15 mL, 0.20 M) and probe **MP-1** (30 μL, 0.50 mM) were added to the vial and carefully mixed. The final concentrations of probe **MP-1**, analyte, and PBS in the solution (3.0 mL) were 5.0 μM, 100 μM, and 10 mM, respectively. Error bars were presented using the standard deviation of a triplicate measurement.

© 2022 The Author(s). Published by the Royal Society of Chemistry

Open Access Article. Published on 24 August 2022. Downloaded on 2/11/2026 12:12:11 PM.
This article is licensed under a Creative Commons Attribution-NonCommercial 3.0 Unported Licence.

2.4 Investigation of Hg^{2+} sensing mechanism

Probe **MP-1** (31 mg, 100 μmol) was dissolved in acetonitrile (10 mL). Mercury(II) perchlorate (80 mg, 200 μmol) was dissolved in DI water (10 mL) and carefully mixed with the prepared solution. The Hg^{2+} signaling progress of **MP-1** was observed by TLC measurement. After the reaction was completed, the mixture was acidified using 0.1 N HCl solution, and the signaling product was extracted by DCM. The volatiles were removed, and the residue was purified by column chromatography (silica gel, eluent: DCM/methanol = 9 : 1, *v*/*v*). The purified Hg^{2+} sensing product was characterized by mass spectral data.

2.5 HPLC analysis of Hg^{2+} signaling product

Sample solutions of **MP-1** only, **MP-1** + Hg^{2+}, and standard resorufin sodium salt were prepared using a pH 7.4 PBS solution containing 20% acetonitrile. The **MP-1** (or resorufin sodium salt) and Hg^{2+} ions were in the sample solutions at final concentrations of 5.0 μM and 100.0 μM, respectively. The HPLC experiment was performed using 50% aq. acetonitrile as the eluent and the C18 reverse phase column (SunFire, 4.6 × 150 mm). The sample injection volume was 20 μL, and the flow rate was 1.0 mL min^{-1}. The column oven was maintained at room temperature, and the HPLC results were obtained with a UV detector (A_{254}).

2.6 Hg^{2+} analysis of artificial urine samples

The Hg^{2+} analysis of the artificial urine samples was conducted in 2-fold diluted artificial urine-based analytical solutions. The artificial urine solution (Sigmatrix Urine Diluent) consisted of $CaCl_2$, $MgCl_2$, KCl, NaCl, NaH_2PO_4, Na_2SO_3, urea, and creatinine, with NaN_3 as a preservative. The sample solution was prepared *via* the addition of DI water (0.75 mL), acetonitrile (540 μL), PBS (150 μL, 0.20 M), artificial urine solution (1.5 mL), and Hg^{2+} ions (0, 0.75, 1.5, 3.0, 6.0, and 9.0 μL, 1.0 mM) in a 15 mL vial. Probe **MP-1** (30 μL, 5.0 mM) was added to the mixture following careful mixing. The final concentrations of **MP-1**, Hg^{2+} ions, and PBS in the 3.0 mL analyte solution were 5.0 μM, 0–3.0 μM, and 10 mM, respectively. The Hg^{2+} calibration curve in the artificial urine solution was obtained by measuring the absorbance ratio (A_{576}/A_{457}) and the ratio of red channel/green channel (*Red*/*Green*) level of the sample images as a function of [Hg^{2+}].

3. Results and discussion

The Hg^{2+}-selective probe was designed considering the selective and mild deprotection capabilities of the phosphinothioate protection group as a signaling switch. Phosphinothioate groups have been effectively used for the protection of phenolic functions and are easily deprotected under mild conditions *via* Hg^{2+}- and F^--induced hydrolysis reactions.[40–43] Resorufin was selected as the signaling fluorochrome because of its well-established chromogenic and fluorogenic responses toward various analytes through the analyte-induced regeneration of the parent dye.[47] The designed probe **MP-1** was easily prepared by the reaction of resorufin sodium salt with dimethylthiophosphinoyl chloride in DMF (yield: 82%) (Scheme 1). The probe structure was characterized by ^{1}H NMR, ^{13}C NMR, and mass spectral data. In its ^{1}H NMR spectrum, four split resonances of characteristic $^nJ_{P-H}$ couplings were perceived for CH_3 (13.5 Hz) and hydrogens of the resorufin moiety (0.7–1.6 Hz), owing to the couplings with the phosphorous atom of the dimethylphosphinothioate moiety. In the ^{13}C NMR spectrum of **MP-1**, seven split resonances with characteristic $^nJ_{P-C}$ couplings were observed for CH_3 (71.7 Hz) and carbons of the resorufin moiety (1.4–9.4 Hz), due to the coupling with the phosphorous atom of the dimethylphosphinothioate moiety.[48]

The selective signaling behavior of the probe was assessed by UV-vis and fluorescence spectroscopy. A 'bird's-eye' view of the possible changes induced by the target analyte was obtained by measuring the spectral properties of the two relevant species of the designed signaling process, namely, probe **MP-1** and its postulated signaling product resorufin **1** (*vide infra*). The two species showed quite contrasting spectral behaviors in an optimized condition of the PBS solution (pH 7.4) containing 20% acetonitrile. Probe **MP-1** showed a strong absorption band at 457 nm in the UV-vis spectrum, while the expected signaling product **1** revealed a notably red-shifted and hyperchromic band at 576 nm (Fig. S1a, ESI†). The solution color changed from light yellow to pink. Meanwhile, probe **MP-1** revealed a weak emission at 587 nm in the fluorescence spectrum under the same conditions, and the solution appeared nearly dark under illumination with a UV lamp (λ_{ex} = 365 nm) (Fig. S1b, ESI†). Conversely, the expected signaling product **1** exhibited a strong emission at 592 nm with intense red fluorescence under the same UV illumination.

Firstly, we observed the UV-vis absorbance of probe **MP-1** in the presence of representative thiophilic metal ions, such as Hg^{2+}, Cu^{2+}, and Ag^+ ions. Probe **MP-1** revealed prominent Hg^{2+} signaling behavior with moderate Cu^{2+} interference (Fig. S2, ESI†). To obtain exclusive Hg^{2+} selectivity of the probe, we employed a citrate additive as a masking agent for interfering Cu^{2+} ions in the measurement solutions.[49] In this condition, the selective response of the probe toward targeting Hg^{2+} ions over common metal ions was elucidated (Fig. 1). Upon the treatment of **MP-1** solution with various metal-containing analytes, only Hg^{2+} induced a marked color change from yellow to pink, which is a characteristic color of the resorufin fluorochrome (Fig. 1, inset). The absorbance enhancement of the probe at 576 nm (A/A_0)$_{576}$ was 63.4-fold. Most of the other tested metal ions revealed insignificant spectral changes; the ratio (A/A_0)$_{576}$ varied in a narrow range between 0.97 for Pb^{2+} and 1.67 for K^+. Since **MP-1** revealed considerable residual absorbance at 457 nm in the PBS solution (pH 7.4) containing 20% (*v*/*v*) acetonitrile, the selectivity toward Hg^{2+} ions was assessed through ratiometric treatment of the signaling data using two relevant absorbances at 576 and 457 nm. The ratio A_{576}/A_{457} was 34.8 for Hg^{2+} and

Scheme 1 Preparation of dimethylphosphinothioate-based probe MP-1.

Open Access Article. Published on 24 August 2022. Downloaded on 2/11/2026 12:12:11 PM.
This article is licensed under a Creative Commons Attribution-NonCommercial 3.0 Unported Licence.

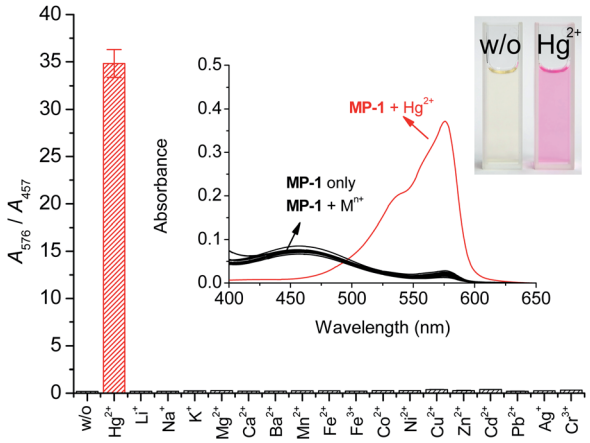

Fig. 1 Changes in absorbance ratio (A_{576}/A_{457}) of **MP-1** in the presence of common metal ions. [**MP-1**] = 5.0 μM, [Hg^{2+}] = [M^{n+}] = 100 μM, [citrate] = 5.0 mM, [PBS 7.4] = 10 mM in aqueous solution containing 20% (*v*/*v*) acetonitrile. Number of measurements (*n*) = 3.

nearly constant for the rest of the metal ions (0.19–0.38) (Fig. 1). Ratiometric analysis revealed that the enhancement of the ratio A_{576}/A_{457} reached 190-fold (0.19 for **MP-1** only and 34.8 for **MP-1** with Hg^{2+} ions). We also confirmed that probe **MP-1** exhibited nearly perfect selectivity toward Hg^{2+} ions over common anions (Fig. S3, ESI†). The ratio A_{576}/A_{457} for anions varied within a narrow range between 0.19 for Cl^- and 0.25 for SO_4^{2-} ions.

Next, the effect of foreign ions on the Hg^{2+} signaling of the probe was assessed to check the practical applicability. The Hg^{2+} signaling was not affected by the presence of commonly encountered metal ionic species. In the presence of background metal ions, the ratio (A_{576}/A_{457}) of the analytes after Hg^{2+} signaling by probe **MP-1** changed marginally between 93.7% (for Cu^{2+}) and 100.1% (for Mn^{2+}) (Fig. 2). Similarly, the probe's Hg^{2+} signaling was not affected by the presence of commonly encountered anionic species (Fig. S4, ESI†).

Probe **MP-1** showed negligible changes in UV-vis absorption behavior up to pH 8 (Fig. 3). Contrastingly, the absorbance ratio (A_{576}/A_{457}) of the Hg^{2+} signaling solution of **MP-1** increased markedly from pH 5 and plateaued at around pH 8. The pH profile of Hg^{2+} signaling behavior by **MP-1** (**MP-1** + Hg^{2+}) matched that of signaling product **1** exactly in the presence of Hg^{2+} ions (**1** + Hg^{2+}). From this result, we hypothesized that the Hg^{2+} signaling pH profile was due to the pH dependency of the absorption property of resorufin **1**, rather than the pH-dependent Hg^{2+} signaling reaction by **MP-1**. Therefore, we chose the PBS solution (pH 7.4) as the working condition for the signaling experiments.

Next, the fluorogenic properties of the probe toward metal ions and anions were measured under the same optimal conditions. Probe **MP-1** exhibited a weak emission at 587 nm under the measuring conditions (Fig. 4). Upon treatment with common metal ions, only Hg^{2+} induced a large increase in the emission band at 592 nm (I/I_0 = 24.4). The remaining metal ions revealed no measurable fluorescence changes; I/I_0 = 0.86 (for Pb^{2+}) – 1.60 (for Ag^+). The other tested thiophilic metal ions did not exhibit concerning responses under the measuring conditions. Moreover, probe **MP-1** showed no measurable changes in fluorescence emission toward commonly encountered anions either; I/I_0 = 0.87 (for S^{2-}) – 1.60 (for F^-) (Fig. S5, ESI†). These observations clearly demonstrated the potential of **MP-1** for the selective analysis of Hg^{2+} ions in common chemical and environmental applications. However, the maximum signal enhancement expressed by the fluorometric enhancement I/I_0 was rather small compared to the colorimetric results (I/I_0 = 24.4 for fluorometry *vs.* $(A_{576}/A_{457})/(A_{576}/A_{457})_0$ = 190 for colorimetry). This is due to the considerable residual fluorescence of probe **MP-1** alone at 592 nm. Therefore, we investigated the colorimetric signaling behavior of probe **MP-1**, which results in more contrasting signaling and enables analysis with the more advantageous ratiometric approach.

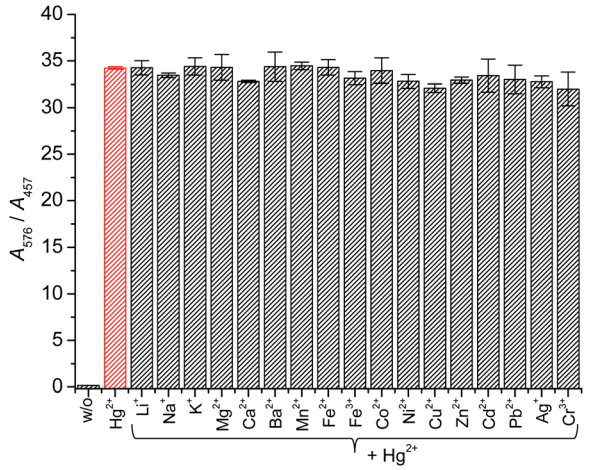

Fig. 2 Changes in absorbance ratio (A_{576}/A_{457}) of Hg^{2+} signaling by **MP-1** in the presence of common background metal ions. [**MP-1**] = 5.0 μM, [Hg^{2+}] = [M^{n+}] = 100 μM, [citrate] = 5.0 mM, [PBS 7.4] = 10 mM in aqueous solution containing 20% (*v*/*v*) acetonitrile. Number of measurements (*n*) = 3.

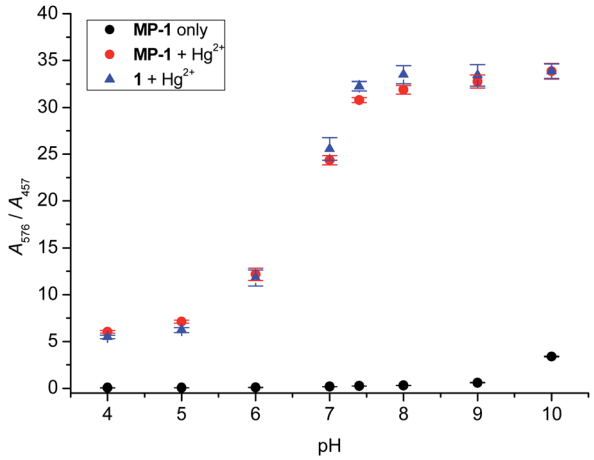

Fig. 3 Effect of pH on Hg^{2+} signaling of **MP-1** expressed by changes in absorbance ratio (A_{576}/A_{457}). [**MP-1**] = [**1**] = 5.0 μM, [Hg^{2+}] = 100 μM, [citrate] = 5.0 mM, [PBS 7.4] = 10 mM in aqueous solution containing 20% (*v*/*v*) acetonitrile. The pH of the solution was adjusted by the addition of 1 N HCl or NaOH. Number of measurements (*n*) = 3.

© 2022 The Author(s). Published by the Royal Society of Chemistry

Open Access Article. Published on 24 August 2022. Downloaded on 2/11/2026 12:12:11 PM.
This article is licensed under a Creative Commons Attribution-NonCommercial 3.0 Unported Licence.

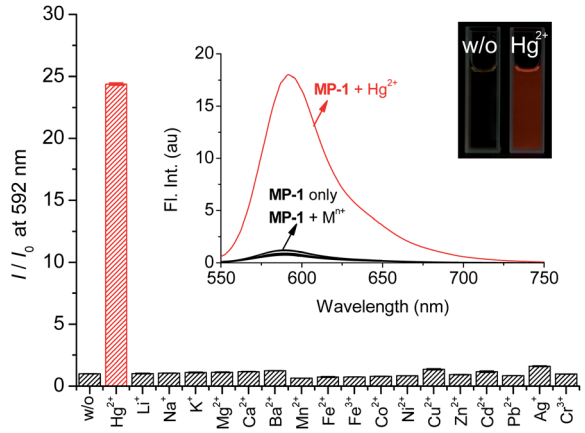

Fig. 4 Changes in fluorescence intensity at 592 nm of **MP-1** as plotted by intensity ratio I/I_0 in the presence of metal ions. [**MP-1**] = 5.0 μM, [Hg^{2+}] = [M^{n+}] = 100 μM, [citrate] = 5.0 mM, [PBS 7.4] = 10 mM in aqueous solution containing 20% (*v*/*v*) acetonitrile. λ_{ex} = 492 nm. Number of measurements (*n*) = 3.

The signaling route could be described by the Hg^{2+}-assisted hydrolysis of the phosphinothioate protecting group of probe **MP-1** to yield parent resorufin fluorochrome **1** (Scheme 2). The proposed sensing mechanism illustrates that the first step is conceived to be the complex formation process between the sulfur atom of the phosphinothioate group and thiophilic Hg^{2+} ions. The thus-formed complex hydrolyzed smoothly to yield resorufin dye and dimethylphosphinic acid as a byproduct, with the concomitant revival of the characteristic absorption and fluorescence signals. The postulated signaling reaction was ascertained by the NMR and mass measurements alongside HPLC monitoring. Upon treatment of probe **MP-1** with Hg^{2+}, the solution turned rapidly pink and revealed intense red fluorescence. The signaling reaction product between **MP-1** and Hg^{2+} was characterized by NMR and mass spectral data. In the ^{1}H NMR spectrum, probe **MP-1** revealed six resonances of the resorufin moiety protons with typical splitting owing to J_{P-H} couplings (Fig. 5). Alternatively, the reaction mixture (**MP-1** + Hg^{2+}) showed three resonances ascribable to resorufin **1** with no extra coupling due to J_{P-H} couplings. In addition, as shown in Fig. S6 (ESI†), in the presence of Hg^{2+} ions, the resonance of methyl protons of the dimethylphosphinothioate moiety of probe **MP-1** at 2.11 ppm disappeared, and a new doublet peak, which is ascribable to the resonance of the methyl protons of

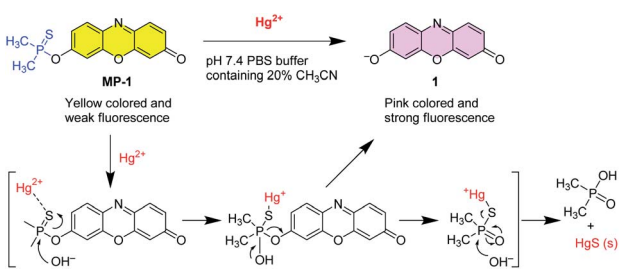

Scheme 2 Proposed Hg^{2+} signaling mechanism by deprotection of probe **MP-1**.

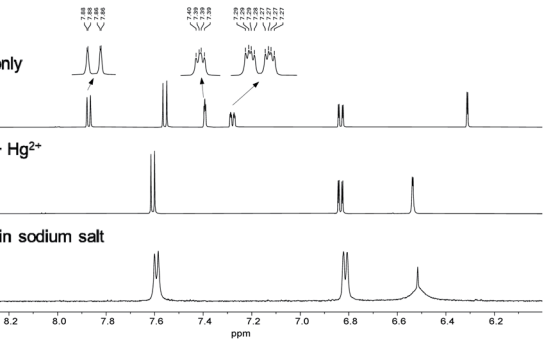

Fig. 5 Partial ^{1}H NMR spectrum of (a) **MP-1**, (b) **MP-1** + Hg^{2+}, and (c) resorufin sodium salt in DMSO-d_6. [**MP-1**] = [resorufin sodium salt] = 5.0 mM. For (b), the spectrum (**MP-1** + Hg^{2+}) was obtained using a mixture of **MP-1** (5.0 mM) and $Hg(ClO_4)_2$ (10.0 mM) in DMSO-d_6.

the byproduct dimethylphosphinic acid,[50] at 1.32 ppm emerged. The mass spectrum of the purified signaling product confirmed a diagnostic peak at m/z = 213.1, which is in agreement with the calculated mass (calculated for $C_{12}H_7NO_3$, 213.0) of signaling product **1** (Fig. S7, ESI†). Moreover, HPLC analysis provided additional supporting evidence. In the presence of Hg^{2+} ions (**MP-1** + Hg^{2+}), the elution time peak for probe **MP-1** at 4.03 minutes disappeared, and a new peak evolved at 1.53 minutes for the reference compound **1** (Fig. S8, ESI†).

The quantitative analytical behavior of **MP-1** for Hg^{2+} determination was studied by UV-vis titration (Fig. 6). The changes in the absorbance ratio (A_{576}/A_{457}) were linearly correlated with the increases in [Hg^{2+}] (R^2 = 0.9987). The limit of detection obtained from the concentration-dependent data as per the IUPAC recommendation ($3s_{blk}/m$) was 12 nM. In addition, we confirmed that the signaling was complete within 5 minutes (Fig. S9, ESI†).

With this background, we tested the practical applicability of the probe for the easy determination of clinically relevant urinary mercury levels. Currently, the Hg^{2+} concentration in urine samples is determined by complicated instruments, such as inductively coupled plasma mass spectrometers and atomic

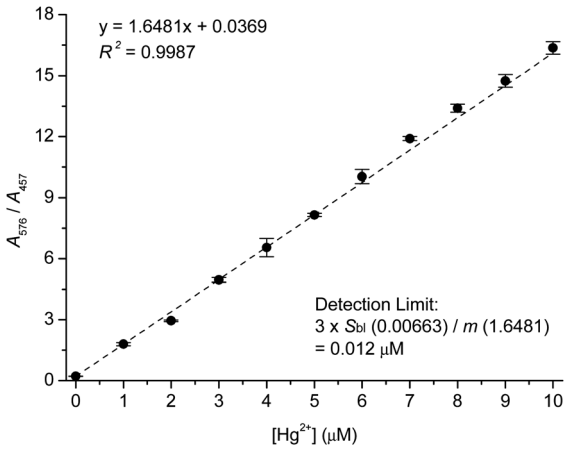

Fig. 6 Calibration curve for UV-vis titration of **MP-1** with Hg^{2+}. [**MP-1**] = 5.0 μM, [Hg^{2+}] = 0–10 μM, [citrate] = 5.0 mM, [PBS 7.4] = 10 mM in aqueous solution containing 20% (*v*/*v*) acetonitrile. Number of measurements (*n*) = 3.

© 2022 The Author(s). Published by the Royal Society of Chemistry

Open Access Article. Published on 24 August 2022. Downloaded on 2/11/2026 12:12:11 PM.
This article is licensed under a Creative Commons Attribution-NonCommercial 3.0 Unported Licence.

absorption spectrometers. We presumed that one could diagnose elevated mercury levels in urine by applying probe **MP-1** without resorting to these expensive and complicated instruments. Subsequently, the interference from major urine components was elucidated. Indeed, most of the metal ionic and anionic constituents showed no interference at all (Fig. 2 and S4, ESI†). Therefore, we measured the possible interference from other urine components of urea and creatinine. As shown in Fig. S10 (ESI†), there were no meaningful responses from these constituents, and the Hg^{2+} signaling of **MP-1** was not disturbed by the presence of the two tested urine ingredients. Thus, the UV-vis titration of **MP-1** with Hg^{2+} in artificial urine (Sigmatrix Urine Diluent) was performed to further elucidate the quantitative signaling potential of the probe. It is known that the Hg^{2+} levels in healthy human urine are less than 5 ng mL^{-1}.[8] Moreover, the facts that a urinary mercury concentration over 100 ppb (0.24 μM) induces neurological symptoms and that one above 800 ppb (1.96 μM) causes death are clinically important.[12] The potential for the probe to diagnose these two clinically important levels was tested by conducting Hg^{2+} concentration-dependent experiments under the same conditions, except employing the 2-fold diluted commercially available artificial urine where no turbidity problem was observed. The calibration curve of Hg^{2+} analysis in artificial urine by probe **MP-1**, as plotted by the absorbance ratio (A_{576}/A_{457}), revealed a good linear relationship up to 3.0 μM (R^2 = 0.9962) (Fig. S11, ESI†). The results showed that **MP-1** could readily signify the fatal level (>800 ppb in urine) and even the neurological symptom level (>100 ppb in urine) for Hg^{2+} intoxication cases.

The colorimetric analytical behavior of **MP-1** could be conveniently monitored by a scanner as a readily available detection tool under the same signaling conditions.[51] The color change from yellow to pink of the signaling solutions was evident under the analysis conditions (Fig. 7a) and could be quantified by the changes in the green channel level as a function of the analytes' [Hg^{2+}]. The correlation plot between the green channel level and [Hg^{2+}] provided a good calibration curve (R^2 = 0.9962) (Fig. S12, ESI†). Meanwhile, other color channel levels (red and blue) did not show meaningful changes with the increases in [Hg^{2+}]. We also tried to obtain a more reliable approach for the assessment of these clinically important Hg^{2+} levels by employing the ratiometric analysis using the ratio of the two-color channel levels. Among these, the ratio between the red and green channel levels, *Red*/*Green*, afforded another useful calibration plot (R^2 = 0.9974) (Fig. 7). The detection limit was calculated to be 91 nM. With this plot, the rapid and accurate diagnosis of fatal and even neurological symptom levels of Hg^{2+} intoxication cases, which were marked in red and blue, respectively, could be readily realized. From these results, we confirmed that the employed analytical technique could be applicable to the early clinical diagnosis of mercury poisoning cases using a standard UV-vis spectrophotometer or an office scanner.

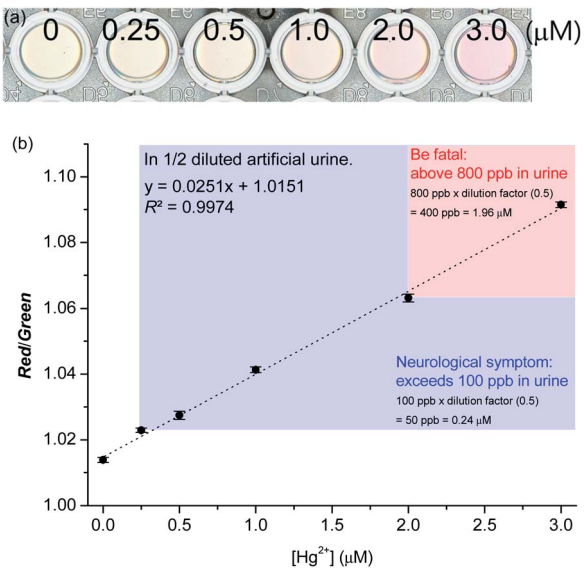

Fig. 7 (a) Scanner image of Hg^{2+} signaling by probe **MP-1** in artificial urine. (b) Calibration curve expressed by *Red*/*Green* channel level of image for Hg^{2+} signaling. [**MP-1**] = 5.0 μM, [Hg^{2+}] = 0–3.0 μM, [citrate] = 5.0 mM, [PBS 7.4] = 10 mM in aqueous solution containing 20% (*v*/*v*) acetonitrile. The regions marked in blue and red indicate the neurological symptom and fatal zones, respectively. Number of measurements (*n*) = 3.

4. Conclusions

We developed a novel Hg^{2+}-selective colorimetric and fluorogenic probe to monitor clinically elevated urinary Hg^{2+} levels. Probe **MP-1** showed the Hg^{2+}-selective signaling behavior owing to the hydrolysis of phosphinothioate protecting group to yield the parent resorufin fluorochrome. Pronounced chromogenic (A_{576}/A_{457} = 190-fold) and fluorescence ($(I/I_0)_{592}$ = 24.4-fold) responses were observed exclusively toward Hg^{2+} ions over other metal ions and anions. Hg^{2+} signaling was complete within 5 min, and the detection limit was calculated to be 12 nM. In particular, the convenient early diagnosis of fatal (1.96 μM) and even neurological symptom (0.24 μM) levels of Hg^{2+} intoxication cases could be readily realized using a common office scanner. The detection limit for Hg^{2+} ion in artificial urine samples using the office scanner was estimated to be 91 nM. These obtained results could be practically useful for the rapid diagnosis of elevated mercury levels in chronic and acute intoxication cases without resorting to complicated heavy instruments.

Conflicts of interest

There are no conflicts of interest to declare.

Acknowledgements

This research was supported by the Chung-Ang University Graduate Research Scholarship in 2021 (HMK) and the National Research Foundation of Korea (NRF) grant funded by the Korea government (MSIT) (No. 2022R1F1A1072643).

Notes and references

1 A. Hojjati-Najafabadi, M. Mansoorianfar, T. Liang, K. Shahin and H. Karimi-Maleh, *Sci. Total Environ.*, 2022, **824**, 153844.

© 2022 The Author(s). Published by the Royal Society of Chemistry

Open Access Article. Published on 24 August 2022. Downloaded on 2/11/2026 12:12:11 PM.
This article is licensed under a Creative Commons Attribution-NonCommercial 3.0 Unported Licence.

2 H. Karimi-Maleh, H. Beitollahi, P. S. Kumar, S. Tajik, P. M. Jahani, F. Karimi, C. Karaman, Y. Vasseghian, M. Baghayeri, J. Rouhi, P. L. Show, S. Rajendran, L. Fu and N. Zare, *Food Chem. Toxicol.*, 2022, **164**, 112961.
3 R. Guo, in *Cross-Border Resource Management*, Elsevier, Netherlands, 4th edn, 2021, Chapter 10 – Cross-border environmental pollution and human health, pp. 291–337.
4 K. L. Wasewar, S. Singh and S. K. Kansal, in *Inorganic Pollutants in Water*, ed. P. Devi, P. Singh and S. K. Kansal, Elsevier, Netherlands, 2020, Chapter 13 – Process intensification of treatment of inorganic water pollutants, pp. 245–271.
5 G. Bjørklund, M. Dadar, J. Mutter and J. Aaseth, *Environ. Res.*, 2017, **159**, 545–554.
6 T. W. Clarkson, *Crit. Rev. Clin. Lab. Sci.*, 1997, **34**, 369–403.
7 F. D. Natale, A. Lancia, A. Molino, M. D. Natale, D. Karatza and D. Musmarra, *J. Hazard. Mater.*, 2006, **132**, 220–225.
8 K. H. Kim, E. Kabir and S. A. Jahan, *J. Hazard. Mater.*, 2016, **306**, 376–385.
9 P. B. Tchounwou, W. K. Ayensu, N. Ninashvili and D. Sutton, *Environ. Toxicol.*, 2003, **18**, 149–175.
10 P. Kaur, M. Aschner and T. Syversen, *Neurotoxicology*, 2006, **27**, 492–500.
11 K. Eto, H. Tokunaga, K. Nagashima and T. Takeuchi, *Toxicol. Pathol.*, 2002, **30**, 714–722.
12 B. J. Ye, B. G. Kim, M. J. Jeon, S. Y. Kim, H. C. Kim, T. W. Jang, H. J. Chae, W. J. Choi, M. Ha and Y. S. Hong, *Ann. Occup. Environ. Med.*, 2016, **28**, 5.
13 W. Zheng, D. Foucher and H. Hintelmann, *J. Anal. At. Spectrom.*, 2007, **22**, 925–930.
14 T. K. Chan, *Clin. Toxicol.*, 2011, **49**, 886–891.
15 C. Chen, H. Yu, J. Zhao, B. Li, L. Qu, S. Liu, P. Zhang and Z. Chai, *Environ. Health Perspect.*, 2006, **114**, 297–301.
16 M. Rafati-Rahimzadeh, M. Rafati-Rahimzadeh, S. Kazemi and A. Moghadamnia, *Daru, J. Pharm. Sci.*, 2014, **22**, 46.
17 A. Sabouri and S. Nouroozi, *RSC Adv.*, 2016, **6**, 80354–80360.
18 E. Kenduzler, M. Ates, Z. Arslan, M. McHenry and P. B. Tchounwou, *Talanta*, 2012, **93**, 404–410.
19 X. Ding, L. Kong, J. Wang, F. Fang, D. Li and J. Liu, *ACS Appl. Mater. Interfaces*, 2013, **5**, 7072–7078.
20 A. Roda, P. Pasini, M. Mirasoli, M. Guardigli, C. Russo, M. Musiani and M. Baraldini, *Anal. Lett.*, 2001, **34**, 29–41.
21 M. S. Won, Y. J. Bae, S. S. Lee and Y. B. Shim, *Electroanalysis*, 2001, **13**, 1003–1007.
22 M. Saleem, M. Rafiq and M. Hanif, Organic material based fluorescent sensor for Hg^{2+}: A brief review on recent development, in *Reviews in Fluorescence 2016*, ed. C. D. Geddes and J. R. Lakowicz, Springer International Publishing AG, Switzerland, 2017, pp. 275–317.
23 P. Mahato, S. Saha, P. Das, H. Agarwalla and A. Das, *RSC Adv.*, 2014, **4**, 36140–36174.
24 A. Kumar, D. Kumar and M. Chhibber, *ChemistrySelect*, 2020, **5**, 13738–13747.
25 P. Singh and P. Sharma, *J. Photochem. Photobiol., A*, 2021, **408**, 113096.
26 C. Li, Q. Niu, J. Wang, T. Wei, T. Li, J. Chen, X. Qin and Q. Yang, *Spectrochim. Acta, Part A*, 2020, **233**, 118208.
27 H. Tan, Y. Zhang and Y. Chen, *Sens. Actuators, B*, 2011, **156**, 120–125.
28 J. He, H. Zhang, J. Zou, Y. Liu, J. Zhuang, Y. Xiao and B. Lei, *Biosens. Bioelectron.*, 2016, **79**, 531–535.
29 M. Rana, M. Balcioglu, N. M. Robertson, M. S. Hizir, S. Yumakc and M. V. Yigit, *Chem. Sci.*, 2017, **8**, 1200–1208.
30 S. Zhu, Y. Zhuo, H. Miao, D. Zhong and X. Yang, *Luminescence*, 2015, **30**, 631–636.
31 T. Samanta and R. Shunmugam, *Mater. Adv.*, 2021, **2**, 64–95.
32 H. Shuai, C. Xiang, L. Qian, F. Bin, L. Xiaohui, D. Jipeng, Z. Chang, L. Jiahui and Z. Wenbin, *Dyes Pigm.*, 2021, **187**, 109125.
33 E. M. Nolan and S. J. Lippard, *Chem. Rev.*, 2008, **108**, 3443–3480.
34 (*a*) H. N. Kim, M. H. Lee, H. J. Kim, J. S. Kim and J. Yoon, *Chem. Soc. Rev.*, 2008, **37**, 1465–1472; (*b*) J. Hu, X. Yu, X. Zhang, C. Jing, T. Liu, X. Hu, S. Lu, K. Uvdal, H.-W. Gao and Z. Hu, *Spectrochim. Acta, Part A*, 2020, **241**, 118657; (*c*) A. Picard-Lafond, D. Larivière and D. Boudreau, *ACS Omega*, 2020, **5**, 701–711.
35 (*a*) Y. Tang, D. Lee, J. Wang, G. Li, J. Yu, W. Lin and J. Yoon, *Chem. Soc. Rev.*, 2015, **44**, 5003–5015; (*b*) G. Yuan, H. Lv, H. Liu, H. He, Q. Sun, X. Zhang and S. Wang, *Dyes Pigm.*, 2020, **183**, 108674; (*c*) J. Pan, J. Ma, L. Liu, D. Li, Y. Huo and H. Liu, *J. Photochem. Photobiol., A*, 2021, **416**, 113322.
36 (*a*) D. Wu, A. C. Sedgwick, T. Gunnlaugsson, E. U. Akkaya, J. Yoon and T. D. James, *Chem. Soc. Rev.*, 2017, **46**, 7105–7123; (*b*) S. De and G. Das, *Dyes Pigm.*, 2021, **195**, 109659.
37 M. Ueki and T. Inazu, *Bull. Chem. Soc. Jpn.*, 1982, **55**, 204–207.
38 M. Ueki and S. Kozo, *Bull. Chem. Soc. Jpn.*, 1983, **56**, 1187–1191.
39 P. G. M. Wuts, in *Green's Protective Groups in Organic Synthesis*, John Wiley & Sons, New Jersey, 5th edn, 2014, p. 540.
40 H. G. Im, H. Y. Kim and S.-K. Chang, *Sens. Actuators, B*, 2014, **191**, 854–859.
41 L. Chen, S. J. Park, D. Wu, H. M. Kim and J. Yoon, *Chem. Commun.*, 2019, **55**, 1766–1769.
42 H. Y. Kim, H. G. Im and S.-K. Chang, *Dyes Pigm.*, 2015, **112**, 170–175.
43 M. Du, B. Huo, J. Liu, M. Li, L. Fang and Y. Yang, *Anal. Chim. Acta*, 2018, **1030**, 172–182.
44 K. Kuwabara, Y. Maekawa and T. Murai, *Tetraherdon*, 2020, **76**, 131152.
45 D. J. Eisler and R. J. Puddephatt, *Inorg. Chem.*, 2006, **45**, 7295–7305.
46 D. D. Perin and B. Dempsey, in *Buffers for pH and Metal Ion Control*, Chapman and Hall Ltd, UK, 1979.
47 M. G. Choi, S. Y. Park, K. Y. Park and S.-K. Chang, *Sci. Rep.*, 2019, **9**, 3348.
48 G. Mavel and M. J. Green, *Chem. Commun.*, 1968, 742–743.
49 E. M. M. Ferreira, R. J. A. L'Amour, J. M. N. Carmo, J. L. Mantovano and M. S. de Carvalho, *Microchem. J.*, 2004, **78**, 1–5.
50 P. V. Ioannou, *Z. Anorg. Allg. Chem.*, 2010, **636**, 1347–1353.
51 D. C. Christodouleas, A. Nemiroski, A. A. Kumar and G. M. Whitesides, *Anal. Chem.*, 2015, **87**, 9170–9178.